

Impact of Channel Correlation on Subspace-Based Activity Detection in Grant-Free NOMA

Bashar Tahir, Stefan Schwarz, and Markus Rupp

Institute of Telecommunications, Technische Universität Wien, Vienna, Austria

Abstract—In this paper, we consider the problem of activity detection in grant-free code-domain non-orthogonal multiple access (NOMA). We focus on performing activity detection via subspace methods under a setup where the data and pilot spreading signatures are of different lengths, and consider a realistic frame-structure similar to existing mobile networks. We investigate the impact of channel correlation on the activity detection performance; first, we consider the case where the channel exhibits high correlation in time and frequency and show how it can heavily deteriorate the performance. To tackle that, we propose to apply user-specific masking sequences overlaid on top of the pilot signatures. Second, we consider the other extreme with the channel being highly selective, and show that it can also negatively impact the performance. We investigate possible pilots' reallocation strategies that can help reduce its impact.

I. INTRODUCTION

Next-generation mobile networks will provide connectivity to a large number of simultaneously accessing devices [1], owing specifically to the expansion of machine-type communication (MTC). As current systems are mainly grant-based, the user equipments (UEs)' access is managed centrally by base stations (BSs). This can cause large control overhead for setting up the connections and high access-latency, when a large number of UEs attempt to access the network simultaneously [2]. In order to address that, grant-free access has been proposed [3], [4]. It allows the UEs to transmit their data on their own, without having to be explicitly scheduled by the BS. However, since the UEs transmit on their own, it can happen that multiple UEs choose to contest the same resources, thus causing a collision of the transmitted packets. At this point, the framework of non-orthogonal multiple access (NOMA) comes into action, as it provides the capability to manage the multi-user interference. The combination, grant-free NOMA, has received wide attention in the literature and has shown the capability to resolve the collisions and support a large number of UEs accessing the network in a grant-free manner [5]–[7].

Since the BS is not aware of which UEs are active at a certain time, it has to perform user activity detection first, before it proceeds with channel estimation and data detection. Given the short-packet nature of MTC traffic and its sporadicity, the subset of UEs active at a certain time is typically smaller than the total number of UEs available. This sparsity has

motivated the application of compressed sensing (CS)-based methods, where the orthogonal matching pursuit algorithm and its extensions have been proposed in the literature, such as in [8], [9]. Another category of algorithms are those based on the estimated sample autocorrelation matrix, where subspace methods, such as MUltiple SIgnal Classification (MUSIC) can be used [10], [11]. In [12] joint activity and data detection using approximate message passing and expectation maximization is proposed. Other algorithms such as expectation propagation has been applied in [13]. Deep learning was also considered for this problem, as in [14].

In this work, we consider activity detection in uplink code-domain NOMA using subspace methods; namely, the MUSIC algorithm. Different from the majority of the mentioned works, we assume that the data and pilots employ different spreading sequences (or signatures). Typically, relatively long sequences are employed for the activity detection and channel estimation in order to support a large number of devices; however, applying these long sequences to the data part can be highly inefficient, as it can substantially reduce the spectral efficiency of the data transmission. Therefore, for the data part we employ short spreading, and the long sequences are only employed for the pilots. Moreover, we apply the activity detection in the context of a frame-structure that is similar to the Long-Term Evolution (LTE)/5th generation (5G) uplink. Our focus is on the impact that the channel correlation has on the performance of activity detection. In the first part, we show that strong time-frequency correlation of the channel can prevent successful detection of the active set of UEs. In order to address that, we propose overlaying the pilot sequences with user-specific masking sequences, which results effectively in a decorrelation of the channel. Then, in the second part, we consider the influence of strong time-frequency selectivity, and show how it can also negatively impact the performance. To manage the strong selectivity, we investigate repositioning the pilot signatures over the time-frequency grid.

II. SYSTEM MODEL

We consider a synchronous code-domain NOMA uplink consisting of a total of K UEs transmitting via orthogonal frequency-division multiplexing (OFDM). We utilize the LTE/5G-like frame-structure depicted in Figure 1, comprising of two resource-blocks (RBs) in time, with each RB consisting of 12 subcarriers and 7 OFDM symbols. The transmitted frame consists of data-blocks resulting from the UE spreading its data-symbols with a spreading signature of length L , and also

Bashar Tahir and Stefan Schwarz are with the Christian Doppler Laboratory for Dependable Wireless Connectivity for the Society in Motion. The financial support by the Austrian Federal Ministry for Digital and Economic Affairs and the National Foundation for Research, Technology and Development is gratefully acknowledged.

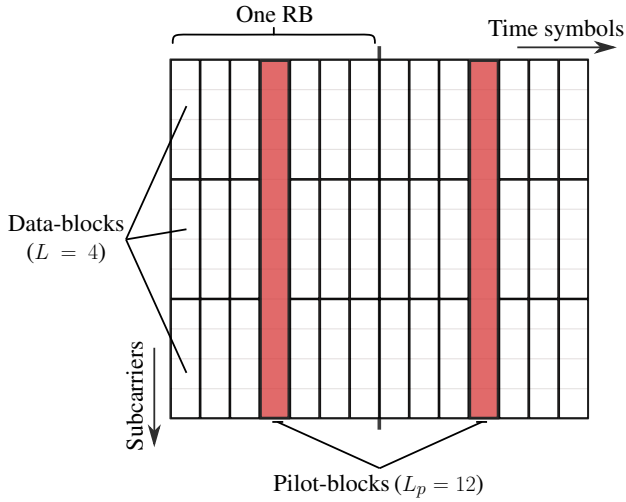


Fig. 1: Considered frame-structure with 12 subcarriers and 14 OFDM symbols.

pilots-blocks, where a pilot signature of length L_p is inserted. Let the number of active UEs at a certain instant be K_a out of K , the received baseband signal at the BS after OFDM demodulation at pilot-block i is given by

$$\mathbf{y}_{p,i} = \sum_{k=1}^{K_a} \sqrt{L_p P_k} \mathbf{a}_k h_{k,i} + \mathbf{n}_{p,i}, \quad i = 1, 2, \dots, B_p, \quad (1)$$

where P_k and $\mathbf{a}_k \in \mathbb{C}^{L_p}$ are the transmit power and pilot signature of UE- k , respectively, $h_{k,i} \in \mathbb{C}$ is the channel coefficient of UE- k at pilot-block i , $\mathbf{n}_{p,i} \in \mathbb{C}^{L_p}$ is the zero-mean Gaussian noise with variance σ_n^2 at pilot-block i , and B_p is the total number of pilot-blocks. Here, for the start, it is assumed that the fading is flat across each pilot-block; hence, it is given as a scalar. Let $\mathbf{A} = [\mathbf{a}_1, \mathbf{a}_2, \dots, \mathbf{a}_{K_a}]$, $\mathbf{h}_i = [\sqrt{L_p P_1} h_{1,i}, \sqrt{L_p P_2} h_{2,i}, \dots, \sqrt{L_p P_{K_a}} h_{K_a,i}]^T$, we can write (1) equivalently as

$$\mathbf{y}_{p,i} = \mathbf{A} \mathbf{h}_i + \mathbf{n}_{p,i}. \quad (2)$$

Under such a system model, the autocorrelation matrix of the received signal over the pilots-blocks (over index i) is

$$\mathbf{R}_{\mathbf{y}_p} = \mathbb{E}\{\mathbf{y}_p \mathbf{y}_p^H\} = \mathbf{A} \mathbf{R}_h \mathbf{A}^H + \sigma_n^2 \mathbf{I}, \quad (3)$$

where $\mathbf{R}_h = \mathbb{E}\{\mathbf{h} \mathbf{h}^H\}$. As can be seen, the autocorrelation matrix consists of two components, corresponding to the signal and noise parts. The idea behind subspace methods is, as long as $0 < K_a < L_p$, then the eigenspace of the autocorrelation matrix can be divided into signal-plus-noise and noise-only subspaces. Based on this, it is possible to tell which signature is active based on how much energy it has in the noise subspace. To elaborate further, consider the eigenvalue decomposition of $\mathbf{R}_{\mathbf{y}_p}$ given by

$$\mathbf{R}_{\mathbf{y}_p} = \mathbf{U} \mathbf{\Lambda} \mathbf{U}^H, \quad (4)$$

with $\mathbf{\Lambda} = \text{diag}(\lambda_1, \lambda_2, \dots, \lambda_{L_p})$ being the matrix of eigenvalues with order $\lambda_1 > \lambda_2 > \dots > \lambda_{L_p}$, and $\mathbf{U} = [\mathbf{u}_1, \mathbf{u}_2, \dots, \mathbf{u}_{L_p}]$ is the matrix of the corresponding eigen-

vectors. Given that K_a UEs are active, the noise subspace \mathbf{U}_n is given by the collection of eigenvectors corresponding to the smallest $L_p - K_a$ eigenvalues, i.e.,

$$\mathbf{U}_n = [\mathbf{u}_{K_a+1}, \mathbf{u}_{K_a+2}, \dots, \mathbf{u}_{L_p}]. \quad (5)$$

The MUSIC spectrum is then calculated as

$$M(k) = \frac{1}{\|\mathbf{U}_n^H \mathbf{a}_k\|^2}, \quad k = 1, 2, \dots, K. \quad (6)$$

The K_a signatures with highest $M(k)$ are then declared active. In practice, we do not have access to the true autocorrelation matrix, but rather we estimate it from the received pilot-blocks. The sample autocorrelation matrix is calculated as

$$\hat{\mathbf{R}}_{\mathbf{y}_p} = \frac{1}{B_p} \sum_{i=1}^{B_p} \mathbf{y}_{p,i} \mathbf{y}_{p,i}^H. \quad (7)$$

If multiple receive antennas are available at the BS, then this estimate can be further improved by averaging over the pilot-blocks from all of the receive antennas.

A. Estimation of K_a

In order to determine the noise subspace in (5) and pick the strongest K_a signatures from (6), we need to know K_a a priori; however, that is not possible in grant-free access, since the BS is not aware of how many UEs are active at a certain time. A similar issue also exists in other activity detection methods, such as in CS, where the sparsity level of the problem needs to be known. Therefore, K_a has to be estimated from the received signal as well, and here, we utilize the Bayesian information criterion (BIC) [15], [16]. Note that BIC has been applied for NOMA activity detection in [10]. Compared to that work, we formulate it here for the case where the noise power is known at the BS, in a fashion similar to [17]. Under the assumption of zero-mean received signal and the samples being i.i.d, the BIC for K_a active UEs is given by [17]

$$\text{BIC}(K_a) = B_p \sum_{k=1}^{L_p} \left(\frac{\hat{\lambda}_k}{\bar{\lambda}_k} + \ln \bar{\lambda}_k \right) + B_p L_p \ln \pi + \frac{K_a}{2} (2L_p - K_a) \ln B_p, \quad (8)$$

where $\hat{\lambda}_k$ is the k -th eigenvalue of the estimated sample autocorrelation matrix $\hat{\mathbf{R}}_{\mathbf{y}_p}$, and we set $\bar{\lambda}_k$ as

$$\bar{\lambda}_k = \begin{cases} \hat{\lambda}_k, & k = 1, 2, \dots, K_a, \\ \sigma_n^2, & k = K_a+1, \dots, L_p. \end{cases} \quad (9)$$

That is, for the current K_a under investigation, the eigenvalues up to K_a are set equal to their maximum likelihood (ML) estimate which we simply obtain from an eigendecomposition of the sample autocorrelation matrix, while the remaining eigenvalues are supposed to belong to the noise-only subspace and thus are set equal to the known noise power. Our estimate of K_a is then the one that minimizes the BIC, i.e.,

$$\hat{K}_a = \arg \min_{K_a} \text{BIC}(K_a). \quad (10)$$

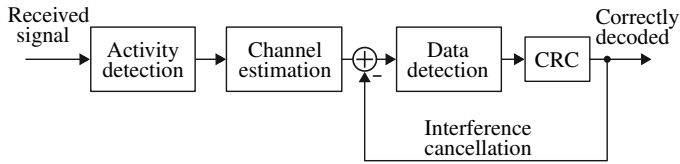


Fig. 2: Receive chain at the BS.

B. Channel Estimation and Data Detection

After finding the active set of UEs, channel estimation and data detection is performed. Let the matrix of estimated active signatures be $\hat{\mathbf{A}}$, the least-squares (LS) channel estimate at pilot-block i is given by

$$\hat{\mathbf{h}}_i = (\hat{\mathbf{A}}^H \hat{\mathbf{A}})^{-1} \hat{\mathbf{A}}^H \mathbf{y}_{p,i}. \quad (11)$$

Once the channel estimates are obtained over all pilot-blocks, linear interpolation (and also extrapolation) is performed to obtain the channel for the whole time-frequency grid.

The BS then proceeds with the data-detection, and in this work, we employ minimum mean square error (MMSE) equalization with parallel interference cancellation (PIC) [18]. Here, the IC is parallel cyclic-redundancy-check (CRC)-based, meaning that all UEs that are decoded and pass their CRC get removed from the received signal. The data detection is then repeated on the cleared-up signal until a maximum number of iterations is reached, or no more UE passes the CRC. The overall receive chain is illustrated in Figure 2.

III. IMPACT OF STRONG TIME-FREQUENCY CORRELATION

The subspace activity detector was formulated under the assumption that the autocorrelation matrix can be divided into distinguished signal-plus-noise and noise-only subspaces. However, in order for this to work, the autocorrelation matrix of the channel coefficients, i.e., \mathbf{R}_h has to be full rank in order for the whole product of $\mathbf{A}\mathbf{R}_h\mathbf{A}^H$ in (3) to have a rank equal to the number of active UEs. To get a full rank \mathbf{R}_h , the channel coefficients across the different pilot-blocks need to be i.i.d., which corresponds to the case where the channel is highly selective from one pilot-block to another; however, typically, the channel is correlated in time and frequency, and therefore neighbouring pilot-blocks, especially in time, are likely to experience a similar channel. In other words, in many situations, the signal received at the pilot-blocks can be highly correlated, and this can be an issue for our detector. To further elaborate on this, let us consider the worst-case scenario where all the UEs undergo flat-fading in both time and frequency. Under such an assumption, we will have $\mathbf{h}_1 = \mathbf{h}_2 = \dots = \mathbf{h}_{B_p} = \mathbf{h}$, i.e., a constant, resulting in $\mathbf{R}_h = \mathbb{E}\{\mathbf{h}\mathbf{h}^H\} = \mathbf{h}\mathbf{h}^H$. The term $\mathbf{h}\mathbf{h}^H$ is simply an outer product of a vector with itself, i.e., a rank-1 matrix. Our resultant autocorrelation matrix is then given by

$$\mathbf{R}_{y_p} = \mathbf{A}\mathbf{h}\mathbf{h}^H\mathbf{A}^H + \sigma_n^2\mathbf{I}. \quad (12)$$

Consequently, the signal part is rank-1; hence, we can only detect one active UE. This can also be observed by looking

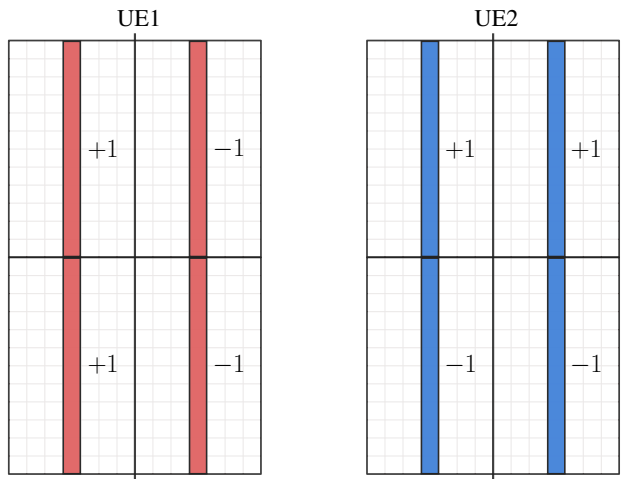


Fig. 3: Masking sequences for two UEs over 4 RBs.

at the sample autocorrelation matrix in (7). If the samples (pilot-blocks) used are correlated, or in a worst-case scenario identical, then it would be a sum of the same outer product, resulting in a rank-1 estimate of the signal part of the autocorrelation matrix. Note that the BIC expression in (8) is derived under an i.i.d. factorization of the likelihood function. Therefore, the correlation between the pilot-blocks also impacts this simplified BIC calculation.

Here, to tackle this issue, we propose the use of masking sequences, applied on top of the pilot-blocks. Figure 3 illustrates the application of masking sequences for UEs transmitting over four RBs, where UE1 transmits with the red pilot signature, while UE2 transmits with the blue one. Instead of transmitting the pilot signatures directly, they are overlaid with a masking sequence. In the considered example, UE1 uses the masking sequences $[+1, +1, -1, -1]$, while UE2 uses $[+1, -1, +1, -1]$. The system model now becomes

$$\mathbf{y}_{p,i} = \sum_{k=1}^{K_a} \sqrt{L_p P_k} \mathbf{a}_k h_{k,i} m_{k,i} + \mathbf{n}_{p,i}, \quad (13)$$

where $m_{k,i}$ is the i -th coefficient of UE- k masking sequence applied at the i -th pilot-block. Let \mathbf{m}_i be the collection of the masking coefficients across the different UEs at block i , then

$$\mathbf{y}_{p,i} = \mathbf{A}(\mathbf{h}_i \circ \mathbf{m}_i) + \mathbf{n}_{p,i}, \quad (14)$$

where \circ denotes the element-wise Hadamard product. Treating the \mathbf{m}_i as a random process across the pilot-blocks, it can be easily shown that the autocorrelation matrix then is given by

$$\mathbf{R}_{y_p} = \mathbf{A}(\mathbf{R}_h \circ \mathbf{R}_m)\mathbf{A}^H + \sigma_n^2\mathbf{I}, \quad (15)$$

where $\mathbf{R}_m = \mathbb{E}\{\mathbf{m}\mathbf{m}^H\}$. Therefore, by designing the masking sequences to be like an i.i.d. process across the UEs, then it would be possible to recover a correct estimation of the signal part of the autocorrelation matrix. For example, even if we have $\mathbf{R}_h = \mathbf{h}\mathbf{h}^H$, the product $\mathbf{h}\mathbf{h}^H \circ \mathbf{R}_m$ can still be full rank if \mathbf{R}_m is full-rank, which is achieved by designing the masking

sequences random-like. One way to design these sequences is to pick them randomly from the alphabet $\{-1, +1\}$, as illustrated in the example of Figure 3. Other designs are also possible, which might enjoy more structure, such as binary Golay sequences [19]. Those masking sequences would be defined in the standard in a similar fashion as the pilot signatures, preferably having a one-to-one correspondence with them. That is, for each pilot signature, there is a corresponding masking sequence.

In the next stage where channel estimation is performed, the effect of employing the masking sequence is removed from the channel estimate. The masking-free estimate is given by

$$\hat{\mathbf{h}}_i = ((\hat{\mathbf{A}}^H \hat{\mathbf{A}})^{-1} \hat{\mathbf{A}}^H \mathbf{y}_{p,i}) \oslash \mathbf{m}_i, \quad (16)$$

where \oslash denotes the element-wise division.

A. Example Scenario with Eight Active UEs

We now evaluate the performance of the activity detection framework with masking sequences. We assume a grant-free system in which the UEs get preconfigured (e.g., with pilot signatures) by the BS during an initial random-access step. Then, for all future transmissions, the UEs transmit on their own when they have data using the preassigned configuration. This prevents collision of the pilots between different UEs.

We consider a scenario where there are $K = 32$ possibly active UEs; however, at a certain time, only $K_a = 8$ UEs are active. They contest a resources' region of 72 subcarriers \times 14 time symbols corresponding to 12 RBs, and the BS employs 2 receive antennas. This brings the number of pilot-blocks that are used to calculate the sample autocorrelation matrix to $B_p = 24$ (12 for each antenna). The task of the receiver is then find the active pilot set, perform channel estimation, and finally equalize the data part and decode it. We consider a scenario with high time-frequency correlation, by assuming a Pedestrian-A channel model, which has a low root-mean-square (RMS) delay spread of 45 ns, and assume the UEs are static and therefore the channel is time-invariant. We assume that there is a pathloss spread of ± 5 dB between the UEs, meaning that the strongest and weakest UEs can have a gap in the receive power of up to 10 dB. Both the data and pilot signatures are from Grassmannian codebooks [20]. As for the masking sequences, we construct them randomly once from $\{+1, -1\}$, and then fix them for all the simulation repetitions. The simulation parameters are summarized in Table I. The various processing operations, such as channel coding, modulation, and channel generation are carried out using the Vienna 5G Link-Level Simulator¹ [21].

Figure 4 shows the average number of correctly decoded UEs using the proposed method versus their average signal-to-noise ratio (SNR) at the BS. The goal here is to have all of the eight active UEs identified and decoded correctly. The perfect activity detection denotes the case where the BS knows exactly which UEs are active, and therefore it only has to

¹Available: <https://www.nt.tuwien.ac.at/research/mobile-communications/vccs/vienna-5g-simulators/>.

Parameter	Value
Active UEs	$K_a = 8$ out of total $K = 32$
Contention region	72 subcarriers \times 14 time symbols
Data signatures	$L = 4$ (4×16 Grassmannian codebook)
Pilots signatures	$L_p = 12$ (12×32 Grassmannian codebook)
Masking sequences	Randomly generated from $\{+1, -1\}$
Receive antennas	$N_R = 2$
Center frequency	2 GHz
Subcarrier spacing	15 kHz
Pathloss spread	± 5 dB
Channel model	Rayleigh, Ped-A (45 ns RMS), velocity = 0
Modulation	4-QAM
Channel coding	Turbo, code-rate 2/3
Activity detection	BIC + MUSIC
Channel estimation	LS with linear inter/extrapolation
Data detection	MMSE-PIC (max. 6 iters)

TABLE I: Simulation parameters for the correlated channels.

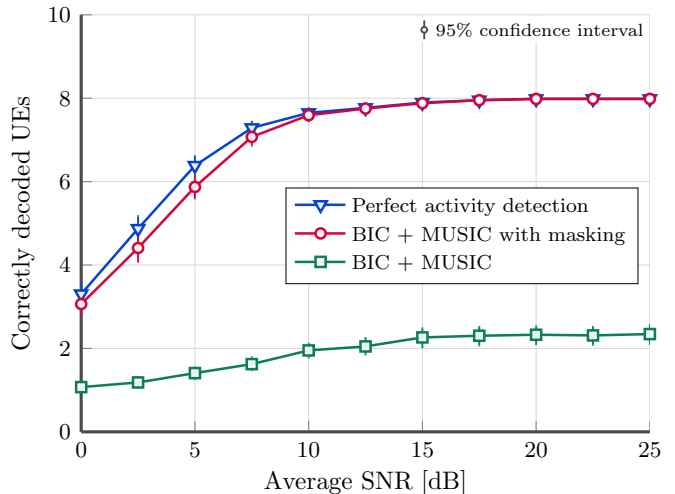
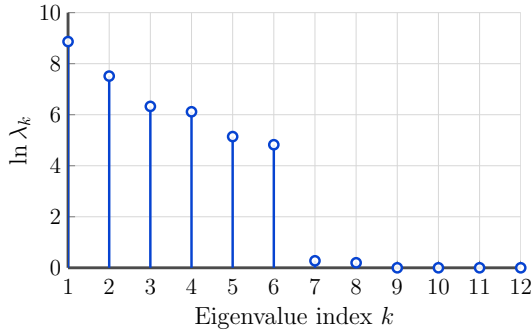


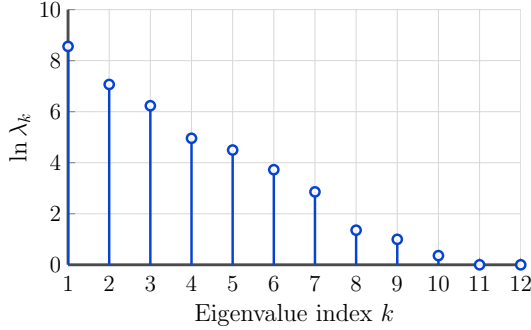
Fig. 4: Activity detection with masking sequences.

perform channel estimation and data detection. This serves as a baseline for our results. As can be seen in the figure, combining the subspace activity detector with the masking sequences results in a performance that is very close to the case with perfect activity detection. When no masking sequences are employed, then due to the correlation of the channel, it is difficult for the signal part to be constructed properly, thus greatly deteriorating the performance.

Note that if the data part was also spread with the same signatures as the pilots, as commonly done in the literature, then in that case, the received signal from the data part can also be utilized in the construction of the sample autocorrelation matrix. As the data symbols can be assumed i.i.d., they would serve a similar function as the masking sequences, allowing the signal part of the autocorrelation matrix to reach the required rank. However, as we mentioned, spreading the data symbols with long sequences can be spectrally inefficient, and therefore we utilize only the pilots for this task, necessitating the application of the masking sequences.



(a) 0 ns RMS delay spread.



(b) 300 ns RMS delay spread.

Fig. 5: Eigenvalues of one realization of $\hat{\mathbf{R}}_{\mathbf{y}_p}$ over a TDL-C channel for $K_a = 6$ and $L_p = 12$.

IV. IMPACT OF STRONG SELECTIVITY

In the previous section, we discussed the benefit of having a selective channel, as it can reduce the correlation between the received signal at the pilot-blocks, which in turn can improve the detection performance. However, since our transmission is sequence-based, we require the channel to be flat within the spreading interval. Therefore, if the channel is too selective, then our system model would not hold anymore, since different parts of the sequence would experience different channel conditions. This modification of the pilot signature changes from one pilot-block to another, and also it is different for the different UEs. Under such conditions, the eigenstructure of the autocorrelation matrix no longer reflects the activity of the pilot signatures, but rather a modified version of them. The more selective the channel is, the more corrupt the estimated autocorrelation matrix will be. In Figure 5a, the eigenvalues of a realization of the autocorrelation matrix for a tapped-delay-line-C (TDL-C) channel with no selectivity is shown for $K_a = 6$ and $L_p = 12$. A clear distinction can be seen between the signal part and the noise part in terms of the magnitude of the eigenvalues. On the other hand, Figure 5b shows the case with 300 ns RMS delay spread. As can be seen, the subspaces are not very clearly separable, which makes it challenging for our subspace detector.

The easiest solution to the selectivity problem, is to use shorter pilot sequences; however, the shorter the pilot se-

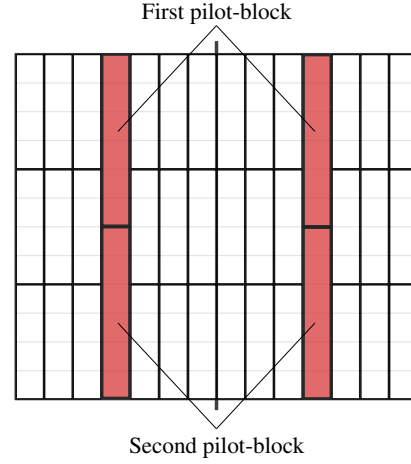


Fig. 6: Splitting the pilot over two blocks in time for $L_p = 12$.

quences are, the smaller is the number of UEs that can be supported. Therefore, we have to keep the pilot sequences long enough, in order to support a sufficient number of connections, while at the same time reduce the impact of selectivity. To that end, we consider here repositioning the pilot-blocks around the RBs. Instead of inserting the pilot sequence along a single RB over 12 consecutive subcarriers, it is split over two neighbouring RBs in time. This is illustrated in Figure 6, where a pilot sequence of length $L_p = 12$ is split over two blocks, each with a length of six. With such a setup, the pilot length in the frequency direction is halved, and therefore less frequency-selectivity is experienced per sub-sequence. The drawback of such an allocation is the worse time-resolution for the channel estimation, since now only a single effective sequence is used to estimate the channel in time.

A. Example Scenario over TDL-C Channels

We investigate the benefit of such an allocation strategy using the same setup of Table I, but we change the channel model to TDL-C with varying RMS delay spread and fix the average SNR of the UEs to 20 dB. The result is shown in Figure 7. There are two factors impacting the performance here. On the one hand, due to the increased frequency-selectivity, the performance of the activity detection deteriorates, as we just explained before. On the other hand, the frequency-selectivity impacts the channel estimation performance as well, i.e., as the channel gets more selective, denser pilots are required in order to be able to track the variations in the channel. As can be seen in the figure, splitting the pilot sequence provides gains for both of these issues. The gain for the activity detection can be seen by comparing the performance under BIC + MUSIC, which shows better robustness against the selectivity with the splitting strategy. The channel estimation gain can be clearly seen when comparing the performance under perfect activity detection. In this case, the split strategy offers better frequency resolution, which helps to provide a better estimation of the channel. Therefore, for such grant-free

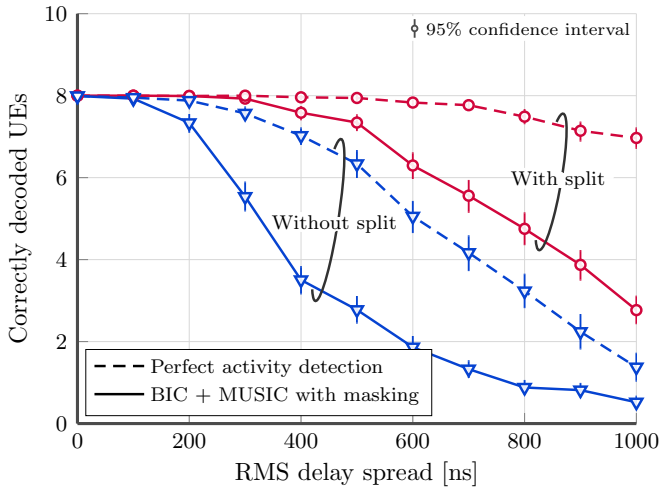


Fig. 7: Detection performance over a frequency-selective channel with $K_a = 8$.

NOMA systems, having the pilot sequences split over multiple OFDM symbols might be a good design approach, in order to avoid the aforementioned problems with frequency-selectivity. Of course, this comes at the cost of decreased robustness to time-selectivity. If time-selectivity is an issue, then one solution is to allocate more OFDM symbols to the pilots. For example, the 5th and 12th OFDM symbols would hold pilot-blocks as well, and then the split can occur over neighbouring OFDM symbols only, leading to less time-variation within the split-block. The disadvantage of doing so is a lower data transmission rate.

Finally, it is important to mention that the setup we considered here is a worst-case scenario in which the channels of all the UEs are suffering from high selectivity. This might not be the case in practice. Also, per 3GPP [22], 300 ns is already considered a long delay spread, and they declare the nominal delay spread to be 100 ns. Thus, above 400 ns would represent extreme cases. Under moderate conditions, the deterioration in performance may not be severe then, especially when combined with those splitting strategies.

V. CONCLUSION

We investigate the impact of channel correlation on activity detection in grant-free NOMA with subspace methods. A setup with a practical frame-structure and where the data and pilot spreading signatures are of different lengths is considered. In the first part, we show how the high correlation of the channel can heavily impact the activity detection performance at the BS. In order to mitigate its effect, we propose to overlay the pilot signatures with user-specific masking sequences. This results effectively in a decorrelation of the channel and allows for a successful detection. Then, in the second part, we consider the other extreme where the channel is highly selective, and how it can negatively affect the performance. We show that the impact of high selectivity may be mitigated by a proper reallocation of the pilot signatures.

REFERENCES

- [1] M. Giordani, M. Polese, M. Mezzavilla, S. Rangan, and M. Zorzi, "Toward 6G Networks: Use Cases and Technologies," *IEEE Communications Magazine*, vol. 58, no. 3, pp. 55–61, 2020.
- [2] S. Ali, N. Rajatheva, and W. Saad, "Fast Uplink Grant for Machine Type Communications: Challenges and Opportunities," *IEEE Communications Magazine*, vol. 57, no. 3, pp. 97–103, 2019.
- [3] L. Liu *et al.*, "Sparse Signal Processing for Grant-Free Massive Connectivity: A Future Paradigm for Random Access Protocols in the Internet of Things," *IEEE Signal Processing Magazine*, vol. 35, no. 5, pp. 88–99, 2018.
- [4] G. Wunder, P. Jung, and C. Wang, "Compressive random access for post-LTE systems," in *2014 IEEE International Conference on Communications Workshops (ICC)*, 2014, pp. 539–544.
- [5] B. Wang, L. Dai, Y. Zhang, T. Mir, and J. Li, "Dynamic Compressive Sensing-Based Multi-User Detection for Uplink Grant-Free NOMA," *IEEE Communications Letters*, vol. 20, no. 11, pp. 2320–2323, 2016.
- [6] M. B. Shahab, R. Abbas, M. Shirvanimoghaddam, and S. J. Johnson, "Grant-Free Non-Orthogonal Multiple Access for IoT: A Survey," *IEEE Communications Surveys Tutorials*, vol. 22, no. 3, pp. 1805–1838, 2020.
- [7] L. Dai *et al.*, "A Survey of Non-Orthogonal Multiple Access for 5G," *IEEE Communications Surveys Tutorials*, vol. 20, no. 3, pp. 2294–2323, 2018.
- [8] B. Wang, L. Dai, T. Mir, and Z. Wang, "Joint User Activity and Data Detection Based on Structured Compressive Sensing for NOMA," *IEEE Communications Letters*, vol. 20, no. 7, pp. 1473–1476, 2016.
- [9] J. Zhang, Y. Pan, and J. Xu, "Compressive Sensing for Joint User Activity and Data Detection in Grant-Free NOMA," *IEEE Wireless Communications Letters*, vol. 8, no. 3, pp. 857–860, 2019.
- [10] S. M. Hasan, K. Mahata, and M. M. Hyder, "Uplink Grant-Free NOMA With Sinusoidal Spreading Sequences," *IEEE Transactions on Communications*, vol. 69, no. 6, pp. 3757–3770, 2021.
- [11] L. Cheng, L. Liu, and S. Cui, "A Covariance-based User Activity Detection and Channel Estimation Approach with Novel Pilot Design," in *2020 IEEE 21st International Workshop on Signal Processing Advances in Wireless Communications (SPAWC)*, 2020, pp. 1–5.
- [12] C. Wei, H. Liu, Z. Zhang, J. Dang, and L. Wu, "Approximate Message Passing-Based Joint User Activity and Data Detection for NOMA," *IEEE Communications Letters*, vol. 21, no. 3, pp. 640–643, 2017.
- [13] J. Ahn, B. Shim, and K. B. Lee, "EP-Based Joint Active User Detection and Channel Estimation for Massive Machine-Type Communications," *IEEE Transactions on Communications*, vol. 67, no. 7, pp. 5178–5189, 2019.
- [14] W. Kim, Y. Ahn, and B. Shim, "Deep Neural Network-Based Active User Detection for Grant-Free NOMA Systems," *IEEE Transactions on Communications*, vol. 68, no. 4, pp. 2143–2155, 2020.
- [15] G. Schwarz, "Estimating the Dimension of a Model," *The Annals of Statistics*, vol. 6, no. 2, pp. 461–464, 1978.
- [16] P. Stoica and Y. Selen, "Model-order selection: a review of information criterion rules," *IEEE Signal Processing Magazine*, vol. 21, no. 4, pp. 36–47, 2004.
- [17] V. T. Ermolaev, A. A. Mal'tsev, and K. V. Rodyushkin, "Statistical Characteristics of the AIC and MDL Criteria in the Problem of Estimating the Number of Sources of Multivariate Signals in the Case of a Short Sample," *Radiophysics and Quantum Electronics*, vol. 44, no. 12, pp. 977–983, Dec 2001.
- [18] B. Tahir, S. Schwarz, and M. Rupp, "Low-Complexity Detection of Uplink NOMA by Exploiting Properties of the Propagation Channel," in *ICC 2020 - 2020 IEEE International Conference on Communications (ICC)*, 2020, pp. 1–6.
- [19] N. Y. Yu, "Binary Golay Spreading Sequences and Reed-Muller Codes for Uplink Grant-Free NOMA," *IEEE Transactions on Communications*, vol. 69, no. 1, pp. 276–290, 2021.
- [20] B. Tahir, S. Schwarz, and M. Rupp, "Constructing Grassmannian Frames by an Iterative Collision-Based Packing," *IEEE Signal Processing Letters*, vol. 26, no. 7, pp. 1056–1060, 2019.
- [21] S. Pratschner *et al.*, "Versatile mobile communications simulation: the Vienna 5G Link Level Simulator," *EURASIP Journal on Wireless Communications and Networking*, vol. 2018, no. 1, p. 226, Sep. 2018.
- [22] 3rd Generation Partnership Project (3GPP), "Technical Specification Group Radio Access Network; Study on channel model for frequency spectrum above 6 GHz," 3rd Generation Partnership Project (3GPP), TR 38.900, Jun. 2018.